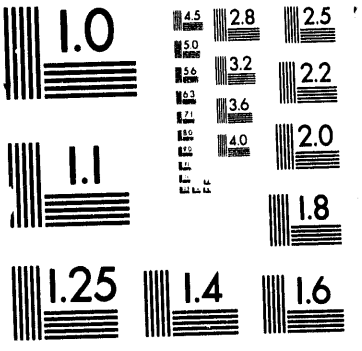
1.0
4.5
2.8
2.5
5.0
3.2
2.2
5.6
6.3
3.6
7.1
4.0
2.0
1.1
1.8
1.25
1.4
1.6

1 of 1

ANL/MSD/CP--81580
Conf-931108--36

ELECTRO-OPTIC MATERIALS BY SOLID SOURCE MOCVD

R. Hiskes,[1] S. A. Dicarolis,[1] J. Fouquet,[1] Z. Lu,[2] R. S. Feigelson,[2]
R. K. Route,[3] F. Leplingard,[4] and C. M. Foster[5]

[1]*Hewlett-Packard Laboratories, Palo Alto, CA 94303*
[2]*Department of Materials Science and Engineering, Stanford University, Stanford, CA 94305-2205*
[3]*Center for Materials Research, Stanford University, Stanford, CA 94305-4045*
[4]*Xerox Palo Alto Research Center, Palo Alto, CA 94304*
[5]*Materials Science Division, Argonne National Laboratory,* Argonne, IL 60439*

December 1993

The submitted manuscript has been authored by a contractor of the U.S. Government under contract No. W-31-109-ENG-38. Accordingly, the U.S. Government retains a nonexclusive, royalty-free license to publish or reproduce the published form of this contribution, or allow others to do so, for U.S. Government purposes.

DISCLAIMER

This report was prepared as an account of work sponsored by an agency of the United States Government. Neither the United States Government nor any agency thereof, nor any of their employees, makes any warranty, express or implied, or assumes any legal liability or responsibility for the accuracy, completeness, or usefulness of any information, apparatus, product, or process disclosed, or represents that its use would not infringe privately owned rights. Reference herein to any specific commercial product, process, or service by trade name, trademark, manufacturer, or otherwise does not necessarily constitute or imply its endorsement, recommendation, or favoring by the United States Government or any agency thereof. The views and opinions of authors expressed herein do not necessarily state or reflect those of the United States Government or any agency thereof.

Presented at the Materials Research Society 1993 Fall Meeting, Symposium on "Metal-Organic Chemical Vapor Deposition of Electronic Ceramics," Boston, MA, November 29-December 3, 1993; to be published in the Proceedings.

*Work supported by the U.S. Department of Energy, BES-Materials Sciences, under contract #W-31-109-ENG-38.

MASTER

DISTRIBUTION OF THIS DOCUMENT IS UNLIMITED

ELECTRO-OPTIC MATERIALS BY SOLID SOURCE MOCVD

R. HISKES[1], S.A. DICAROLIS[1], J. FOUQUET[1], Z. LU[2], R.S. FEIGELSON[2], R.K. ROUTE[3], F. LEPLINGARD[4] and C. M. FOSTER[5]
[1]Hewlett-Packard Laboratories, 3500 Deer Creek Road, Palo Alto, CA 94303
[2]Stanford University, Department of Materials Science and Engineering, Stanford, CA 94305-2205
[3]Center for Materials Research, Stanford University, Stanford, CA 94305-4045
[4]Xerox Palo Alto Research Center, 3333 Coyote Hill Road, Palo Alto, CA 94304
[5]Argonne National Laboratory, 9700 Cass Avenue, Argonne, IL 60439

ABSTRACT

The solid source MOCVD technique[1,2], employing a single powder vaporization source composed of mixed beta-diketonate metalorganic compounds, has been used to grow thin films of a variety of electro-optic materials, including lithium niobate, strontium barium niobate, and potassium niobate. Results for potassium niobate films are quite preliminary, but indicate that a volatile potassium organometallic source can be synthesized which is useful for growing potassium niobate by MOCVD. High quality single phase (001) oriented strontium barium niobate films have been deposited which exhibit waveguiding behavior. The most extensive work has been done on lithium niobate, which has been deposited epitaxially on a variety of substrates. Oriented z-axis (001) films have been grown on c-axis sapphire with and without a (111) oriented platinum base electrode and on a bulk grown lithium niobate substrate. Films grown directly on c-axis sapphire at 700 C exhibit x-ray rocking curve linewidths as low as .044 degrees, nearly perfect in-plane orientation as determined by x-ray phi scans, and peak-to-peak surface roughness less than 40 Å. Optical waveguiding has been demonstrated by a single prism coupling technique on similar films 1175 - 2000 Å thick grown at 500 C, with optical losses of approximately 2 db/cm at 632.8 nm measured over 3.5 cm long films. Polarization vs. electric field measurements on 1100 Å thick films grown on platinum show a hysteresis loop indicating ferroelectric behavior.

INTRODUCTION

Although the beta-diketonate metalorganic complexes were used to successfully grow epitaxial oxide thin films as long ago as 1973[3], interest in this class of metalorganic precursors remained at minimal levels for more than a decade. Intense interest has only recently been rekindled (1987) due to the emergence of the worldwide effort to develop reliable and reproducible thin film deposition techniques for high temperature superconductors, such as yttrium barium copper oxide (YBCO). Many of the heavy metal beta-diketonate complexes, including barium tetramethylheptanedionate ($Ba(thd)_2$), strontium thd and others readily decompose at elevated temperatures. The barium compound, for example, begins to decompose and polymerize almost as rapidly as it volatalizes, even at reduced pressures[4]. Although new classes of more stable compounds have been developed recently[5,6], and techniques implemented which help to stabilize the heavy metal metalorganic complexes in the vapor phase[7], reproducible growth of many of the technologically interesting oxides has often proved difficult by conventional MOCVD, which relies on bubblers containing the metalorganic precursors held at elevated

temperatures for extended periods of time to provide the source vapor. Therefore, we developed the Solid Source Metalorganic Deposition (SSMD) reactor which obviates the precursor stability problem and allows reproducible growth of oxide thin films (on substrates up to 4" in diameter) from these marginally volatile heavy metal diketonate sources..

The SSMD technique has been described previously[1,2]. Initially developed for large area growth of the high temperature superconductor yttrium barium copper oxide, the technique has been extended to include various buffer layers such as CeO_2 and MgO needed for reaction barriers on sapphire substrates, magnetic films including haematite (α-Fe_2O_3) and nickel cobalt oxide ($NiCoO_x$), non-oxides such as the low voltage phosphor CaS doped with terbium (a hybrid process using a liquid sulfur precursor), the superionic conductor gadolinium doped barium cerate (Gd:$BaCeO_3$) for solid-state fuel cell development, low resistivity Au/Cr bilayers on quartz and highly resistive MoO_x films on quartz for mass spectrometer applications, $LaSrCoO_3$ base electrodes for ferroelectric applications, SiO_2 films on silicon for integrated optics, piezoelectric films such as lead zirconate titanate and lead magnesium niobate, and recently the electro-optic materials $LiNbO_3$, $KNbO_3$ and $Sr_xBa_{1-x}Nb_2O_6$. The SSMD reactor is beginning to be used by researchers in other laboratories[5,9,10].

Much of the development work for these materials has been published[1,2,8] or is in the process of being prepared for publication. In this paper, in order to illustrate the power of SSMD, we will describe the reactor, briefly mention the ferroelectrics $Sr_xBa_{1-x}Nb_2O_6$ and $KNbO_3$, and then focus on the growth and properties of the technologically important electro-optic thin film $LiNbO_3$, useful for a variety of applications including waveguides, modulators, and ferroelectric memories.

MOCVD REACTOR DESIGN

The reactor configuration is shown in Figure 1. Metalorganic precursors, most of which are readily available as dry inert powders, are ground together (if necessary) in a mortar and pestle. Although a variety of different ligands are available, we have found it advantageous to use the same ligand for all the sources which must be mixed together prior to use to prevent ligand exchange and subsequent decomposition during volatilization. Most of the oxide thin films to be described were deposited using tetramethylheptanedionate (thd) compounds either prepared in-house or obtained from Strem[11].

The powders are packed into a 4 mm diameter precision bore quartz tube. This tube is closed at the bottom and has a 0.4 mm longitudinal slot along one side to permit easy exit of the vapor as the powder is volatilized. The powder density in the precursor tube can be fixed by packing a known weight of the precursors to a fixed depth in the tube, or it can be readily calculated by measuring both the weight of the tube before and after packing and the height of the powder. This procedure permits accurate control of the growth rate from run to run.

The precursor tube is placed in the U shaped quartz reactor and driven down into a very sharp temperature gradient by a precision screw drive on the outside of the reactor. The drive is magnetically coupled to the precursor tube. The sharp temperature gradient is maintained by a quartz halogen lamp placed directly below a water jacket in the reactor. The reactor is maintained at 1 - 760 torr depending on the materials deposited, and the precursor tube is driven down at rates of 0.1 - 5 mm/min. Each of the constituent powders

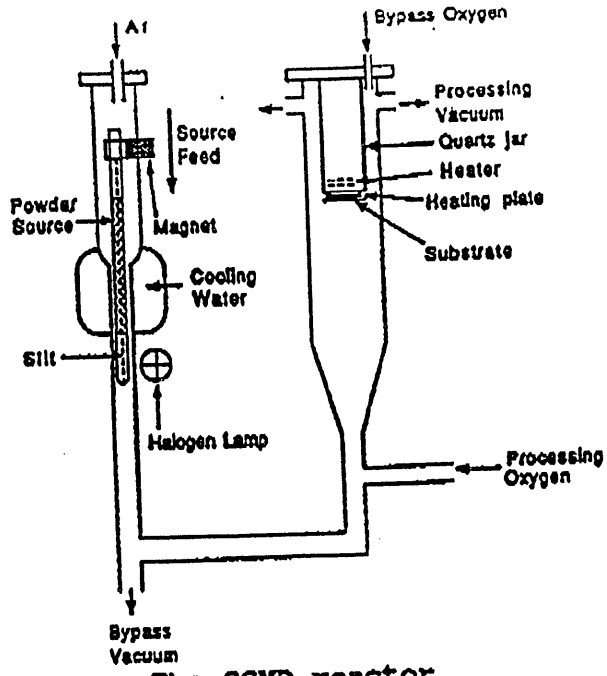

Figure 1. The SSMD reactor.

in a multicomponent mixture vaporizes at its own particular vaporization temperature in the temperature gradient, and as long as the tube velocity is constant, steady state vaporization is obtained and constant vapor composition ensues[10]. The temperature gradient can be as high as 100 °C/mm, and the precursors are vaporized in the hot zone before they can polymerize or decompose.

It takes about 1 second for the vapor to be swept through the reactor to the substrate surface by 300 sccm of argon carrier gas. 300 - 1000 sccm of oxygen for oxide growth or forming gas (4% H_2 in argon) for non-oxides are introduced and mixed with the vapor stream, and laminar flow is maintained by gradually increasing the reactor inside diameter from 14 mm to 200 mm at a 15 degree cone angle. The warm wall reactor is maintained at 150-300 °C by keeping the U shaped portion of the quartz tube in a heated and insulated metal box. Several different modifications of the substrate holder and heating assembly are in use, two of which are described in references 1 and 2. Up to 4" diameter substrates can be accommodated in these reactors. The configuration used for most of the films described here employs a 6" diameter molybdenum disilicide flat (pancake) resistance heater. This heater is quite stable in oxygen atmospheres at temperatures over 1800 C and radiates heat to a 4" nickel susceptor suspended below it. The substrates are mounted in a quartz holder just below the susceptor, but not touching it. Temperature is monitored with a thermocouple embedded in the nickel susceptor, and careful surface measurements of the oxide substrates indicate a 200 C temperature drop between susceptor and the growing film. All temperatures reported in this paper are substrate surface temperatures.

The reactor is held at 1 Torr up to near atmospheric pressure with a roughing pump by adjusting a gate valve in the exhaust line as well as manipulating flows through mass flow controllers. During startup, the bypass exhaust valve is opened while the process vacuum remains closed. After several mm of reactants have vaporized, a steady state vapor composition is obtained. The bypass valve is closed, the process vacuum valve is opened, and film growth begins. Although much of the warm wall reactor is kept at elevated

temperatures, all the flanges and valves are at room temperature, [illegible] exotic seals.

This type of upflow stagnation point reactor inherently produces very uniform film growth since buoyancy and convective effects in the gas stream are minimized[12,13]. The laminar flow (Reynolds number < 1000) results in thin and uniform momentum, thermal and solute boundary layers across the entire area of the substrate, and film growth occurs by diffusion of the reactants and reaction products across this boundary layer from the well mixed vapor in the reaction chamber to the substrate surface. In this way uniform films can be grown across large area substrates. In principle, the area can be extended indefinitely by making the quartz tube larger in diameter and employing a larger diameter heater while adjusting the total gas flows to keep the Reynolds number constant.

The quartz tube permits visual examination of any portion of the reactor during the process. For example, the vapor/solid interface in the precursor tube is visually monitored and its vertical position can be adjusted by changing the power to the vaporizing lamp. Any condensation or pyrolysis at unwanted areas in the reactor is instantly observable, and wall temperatures can be adjusted accordingly.

STRONTIUM BARIUM NIOBATE

We have grown 2000 - 3000 Å thick single phase (001) oriented $Sr_xBa_{1-x}Nb_2O_6$ (SBN) on (100) MgO substrates. Optical waveguiding was demonstrated in these films. The solubility range of the SBN films grown by SSMD is shifted slightly from the solubility range reported for bulk SBN[14] in the direction away from the Nb apex of an isothermal slice through the ternary oxide phase diagram. Further details of this work are reported in the paper by Lu et al[15].

POTASSIUM NIOBATE

Based on an early literature report of a volatile potassium THD compound[16], we synthesized the metalorganic according to the reported procedure, prepared a 50:50 mixture of the potassium and niobium thd powders, and grew one 2000 Å film on c-plane sapphire at 500 C. Theta-two theta x-ray diffraction analysis indicated the film was not entirely phase pure but contained a significant amount of oriented $KNbO_3$, indicating that SSMD can be used for the deposition of epitaxial thin films of $KNbO_3$ with a suitable adjustment of the source composition to a larger K/Nb ratio. This is consistent with a presumed lower sticking coefficient (higher vaporization kinetics) of potassium versus niobium on the film surface. Further work on this system is in progress.

LITHIUM NIOBATE

Although $LiNbO_3$ thin films have been grown by a variety of standard techniques, including sputtering[17], laser ablation[18], LPE[19], MBE[20], and sol-gel[21], there are to our knowledge only two other reports of $LiNbO_3$ grown by MOCVD[22,23]. In the first case the reported optical loss was very high (40 dB/cm), and in the second the loss was not measured. We have grown epitaxial c-axis (+ z direction) $LiNbO_3$ thin films on bare c-

plane sapphire substrates, on epitaxial (111) oriented 500-1000 Angstrom thick Pt buffer layers sputtered on the sapphire substrates, and on bulk c-axis $LiNbO_3$ substrates. The growth rates for these films are in the range 10 to 25 Å/min. The metalorganic precursors $Nb(thd)_4$ and Li(thd) were either prepared according to the synthesis procedures given by Hammond[16], or obtained commercially from Strem[11]. The $Nb(thd)_4$ was found to be quite stable and reproducible from batch to batch whether synthesized at Hewlett-Packard or purchased. However, the quality of the Li(thd) is sensitive to details of the preparation process and both the color (white with yellow overtones) and degree of dryness of the powder varies. This has been found to have a profound effect on the deposition process and quality of the films, and therefore we have used differential scanning calorimetry to look for differences between in-house and commercial powders. The results indicate the commercial Li(thd) is purer, exhibiting only one major peak and one minor peak. The Li(thd) synthesized in-house exhibits an additional peak, is less dry and has less of a yellow cast than the commercial Li(thd). We surmise that the extra peak is due to retained solvent from one of the synthesis steps, and that its effect seems to be to stabilize the Li(thd) against oxidation at higher temperatures in the reactor.

We find it difficult to avoid the formation of a gas-phase-nucleated white powder in the reactor when using commercial Li(thd). X-ray diffraction analysis of this powder indicates it is Li_2CO_3. Substrate surface temperatures higher than 550 C generate so much Li_2CO_3 as the reactants approach the substrate, that the films are often opaque from incorporated particulates. The in-house Li(thd) on the other hand, permits growth higher than 750 C without the formation of this white soot. Adding the neutral thd ligand as a vapor during the growth process with commercial Li(thd) also seems to retard the vapor phase reaction that leads to soot formation. This indicates the source impurity may be retained thd ligand, which inhibits premature oxidation by pushing the chemical equilibrium in the opposite direction.

Higher growth temperatures ($\geq$700 C) lead to improved crystallinity in the films, but also can result in thermal stress induced cracking in films thicker than 1500 Å grown on c-plane sapphire. The higher growth temperatures appear advantageous for homoeptitaxial growth on $LiNbO_3$ substrates, and the lower temperatures ($\sim$500 C) are best for growing thick films on c-plane sapphire for waveguiding applications.

Phase Equilibria and Chemical Characterization

At 950 C, the solid solubility field of the $LiNbO_3$ phase in the pseudo-binary Li_2O-Nb_2O_5 phase diagram[24] spans the compositional range from 47.7 to 50.2 mole percent Li_2O as shown in Figure 2. It decreases to approximately 49.2 to 50.2 mole percent Li_2O at 800 C and appears to narrow rapidly at temperatures lower than 800 C. In SSMD, deposition is carried out at much lower temperatures, particularly on sapphire substrates, and as a result the stoichiometry must be carefully controlled. Outside the single phase existance regime, a $LiNbO_3$ + Li_3NbO_4 two phase region exists on the Li-rich side, and a $LiNbO_3$ + $LiNb_3O_8$ two phase region exists on the Li-poor side. At a growth temperature of 640 C, depending on the exact stoichiometry of the Li(thd) we find that phase pure $LiNbO_3$ can be grown for powder compositions between 65 - 67 mole percent Li as shown in Figure 3, whereas (222) Li_3NbO_4 begins to appear at 70% Li and (220) $LiNb_3O_8$ is present at 60% Li. Homoepitaxial growth of thick films (>1 μm) on $LiNbO_3$ bulk substrates must take place at much higher temperatures, since the composition of the bulk $LiNbO_3$ is fixed by

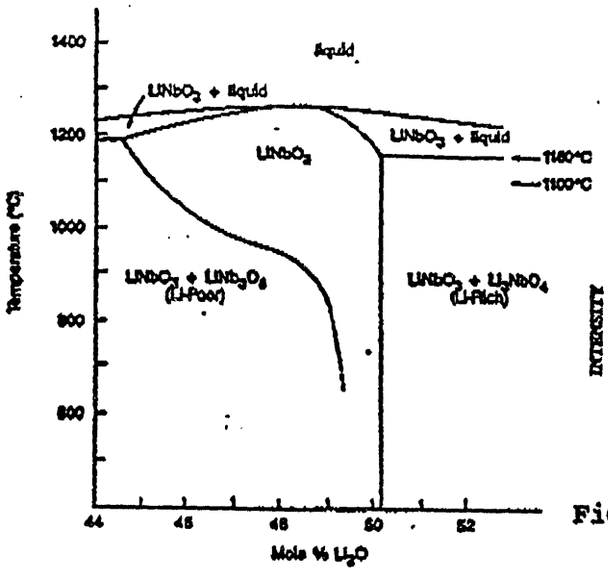

Figure 2. Li_2O-Nb_2O_3 Equilibria.

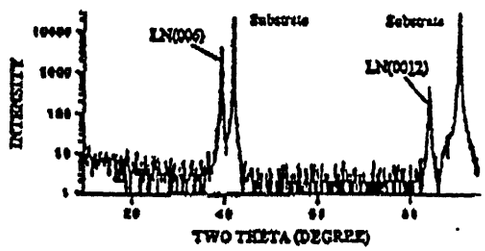

Figure 3. $LiNbO_3$ on c-axis sapphire.

the congruently melting composition shown in Figure 2, and the substrate may start to decompose when held at lower temperatures in the two phase region during the time needed for film growth. However we have grown 2000 Angstrom films on both +z and -z $LiNbO_3$ substrates at 500 - 700 C, and find that substrate decomposition is not yet apparent during the 1 - 2 hour growth runs. The films grow in the +z direction even if the -z face of the substrate is used for film growth. This was readily determined by etching the films in HF, since the +z face etches very slowly while the -z face is etched quite rapidly to a rough surface.

One interesting application for thick films on bulk $LiNbO_3$ substrates is the reduction of cation impurities commonly found in bulk waveguides, which may cause photorefractive damage in the waveguides upon exposure to intense laser illumination. A SIMS scan through a 5000 Angstrom SSMD film into the $LiNbO_3$ substrate revealed that iron, one of the chief culprits implicated in photorefractive damage, is a factor of 30 lower in the film than in the substrate.

Structural Characterization

An XRD off-axis phi scan of the $LiNbO_3$ (012) peak grown at 700 C shows clear three-fold symmetry about the film plane normal as shown in Figure 4, and the peaks coincide exactly with the sapphire substrate (012) peaks, indicating excellent in-plane orientation with [1010]$LiNbO_3$ ||[1010] sapphire. As the growth temperature decreases, more and more 60 degree rotated domains appear as shown in Figure 5. The influence of substrate temperature on other film properties was determined for films grown with a fixed source composition of 65% Li. The results are summarized in Table I. Thicknesses were measured by both Rutherford backscattering (RBS) and by measuring transmission as a function of wavelength with a uv-visible spectrometer. Although RBS cannot detect lithium, the thickness could be determined from the niobium peak by assuming the

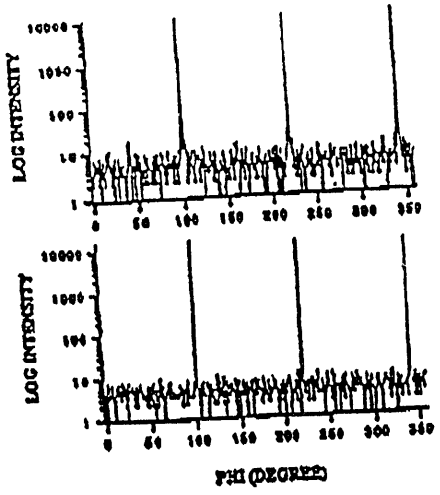

Figure 4. Phi scan for film(top) and Al_2O_3 (bottom).

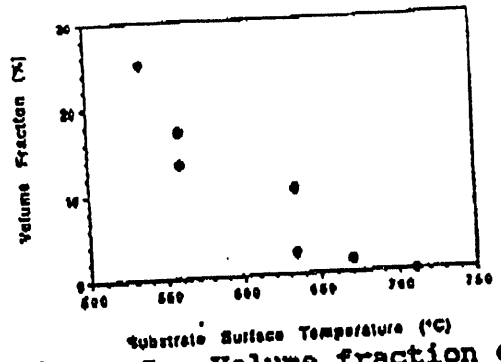

Figure 5. Volume fraction of 60° rotated grains.

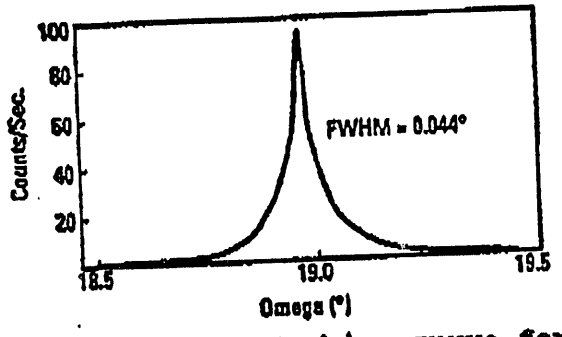

Figure 6. Rocking curve for (006) peak.

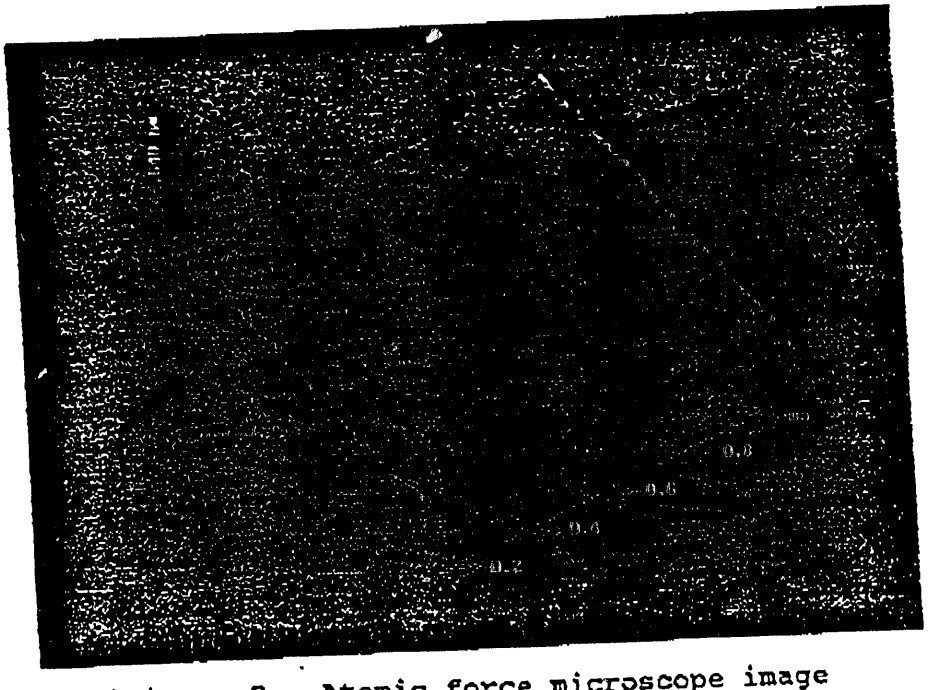

Figure 7. Atomic force microscope image of $LiNbO_3$ film.

stoichiometry. Calculated c-axis lattice parameters are less than the stoichiometric single crystal value of 13.867 Å. The d-spacing of the (012) plane was also measured and found to be slightly larger than the reported bulk value of 3.754 Å. Using the d spacing of the (001) and (012) planes listed in Table I, the a-axis lattice parameters could be calculated and were found to be 5.24, 5.22 and 5.20 Å for films grown at 710, 675 and 640 C respectively. (The accuracy of this calculation is limited by the uncertainty in $d_{(012)}$, and is estimated to be about +0.06 Å.) The a-axis lattice parameters are larger than the single crystal value (5.1478 Å), which suggests the films are under quite a bit of tension at room temperature.

The $LiNbO_3$ (006) rocking curve peak width provides a good indication of film quality since it assesses the spatially averaged out-of-plane misalignment. At a growth temperature of 710 C, a rocking curve FWHM of 0.044 degrees (Figure 6) was obtained on a film grown from a 65% Li source composition, indicating near-perfect out-of-plane alignment. (The sapphire substrate (006) rocking curve FWHM value was 0.007 degrees.). To our knowledge this is the best crystalline quality reported in the literature for a lattice mismatched lithium niobate film. The rocking curve FWHM increases to 0.1 degree as the deposition temperature decreases to 500 C.

The surface morphology of the films as measured by atomic force microscopy was quite smooth as shown in Figure 7 for a 1200 Angstrom film on c-plane sapphire grown at 700 C. The peak-to-peak surface roughness for this film is approximately 40 Å.

Table I. $LiNbO_3$ Film Properties

T_s (°C)	RBS			Spectrometry			d(001) (Å)	d(012) (Å)	Rocking Curve FWHM Value (°)
	Thickness	no	ne	Thickness	no	ne			
710	1022 Å	2.32	2.27	1220 Å	2.24	2.12	13.801	3.79	0.044
675	1162 Å	2.31	2.27	1285 Å	2.27	2.18	13.801	3.78	0.053
640	1190 Å	2.33	2.26	1464 Å	2.25	2.11	13.810	3.77	0.088

Note: error bar for RBS thickness is ±55 Å, for no calculated from RBS thickness is ±0.02, for ne calculated from RBS thickness is ±0.04, for d(001) is ±0.006 Å, for d(012) is ±0.025 Å

Optical Characterization

Optical properties were measured on films deposited on 10 mil thick rectangular c-axis sapphire substrates measuring 1 cm by 4 cm long using a single prism (rutile) coupling technique with a 632.8 nm He-Ne laser. All the films measured were less than 2000 Å thick and therefore supported only one TE and one TM mode. The optical loss was measured here and at Xerox PARC using a silicon photodiode coupled to a traveling optical fiber to measure scatter from the guided mode as a function of distance from the coupling spot, and was also measured at Argonne National Laboratory by imaging the scatter with a CCD camera and extracting loss by image analysis techniques. An early 2000 Å thick film was measured at HP to be 25-30 dB/cm. Upon annealing in oxygen at 400 C for 24 hours the loss dropped to 3-5 dB/cm. Further annealing at 500 C for 18 hours increased the loss to 8-9 dB/cm. This film was then measured at Argonne to be ~8dB/cm (a curve fit of the data yielded 7.75 dB/cm for the TE_0 mode and 7.73 dB/cm for the TM_0 mode.) This particular film was grown in two steps of 1000 Å each and the film was cooled to room temperature between the two growth runs, which may account for the high loss. A number of subsequent films with thicknesses of 1100 to 1400 Å have been

measured both at HP and at Xerox. In these films the guided mode travels to the edge of the 3.75 cm film and losses of approximately 2 db/cm for both the TE_0 and TM_0 modes have been measured. The loss for the TM_0 mode is shown in Figure 8. The reproducibility of the measurement between the three laboratories appears to be about 1 dB/cm. Peaks and valleys in the data in Figure 8 are caused by visually perceptible inhomogeneities in scattered light either in the film or on the film or substrate surface. Annealing one of these low loss films in oxygen at 400 C for three hours significantly increased the scattering instead of decreasing it as in the earlier film. The mechanism for change in optical loss with annealing, also seen by Schwyn[17] for sputtered $LiNbO_3$ films, is not well understood at this time.

From the prism coupling angles, refractive indices were calculated using both RBS and transmission spectra (spectrometer) thickness data and the results are listed in Table I. The transmission spectra thickness values depend on short wavelength data, which are complicated by the fact that accurate refractive indices for wavelengths less than 400 nm are not well known. It was necessary to use extrapolated values calculated from the formula given in[25]. The calculated transmission thicknesses were found to be 10-20% larger than the measured thicknesses. This discrepancy suggests that the refractive indices of the films may slightly different from those measured for bulk single crystals.

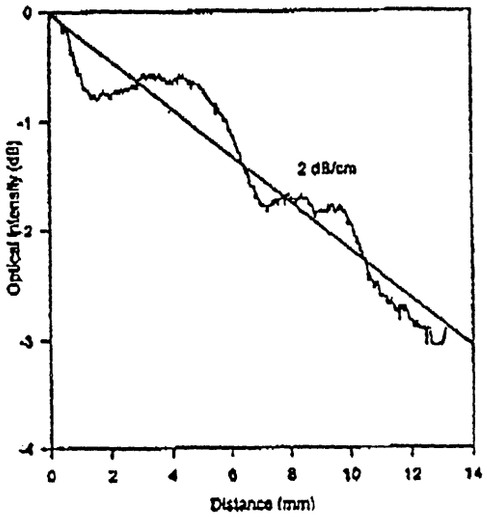

Figure 8. Energy loss for TM_0 mode.

Electrical Characterization

We have grown $LiNbO_3$ films 1000 - 2000 Å thick on sputtered (111) oriented Pt base electrode layers on c-axis sapphire for electrical measurements. An x-ray scan for a 1200 Å thick film (Figure 9) shows nearly 100% c-axis oriention with two unknown impurity peaks. A number of electrical and electro-optic measurements on these films are in progress, including polarization - field hysteresis loops using a Radiant Technologies, Inc. RT66A analyzer[26], and measurements of the electro-optic coefficients. At this time we have preliminary hysteresis loop data. The films clearly exhibit polarization behavior as seen in Figure 9 for an 1100 Å thick film grown at 500 C. The data shown here are the

result of the Analysis Software from Radiant Technologies, Inc., which filters out resistive, and capacitive components from the hysteresis loop. Although the remanent polarization P_r is rather low, it may be consistent for such a thin film which can only be driven at very low voltages before breakdown, but it is more likely that the film properties on Pt are not yet optimized.

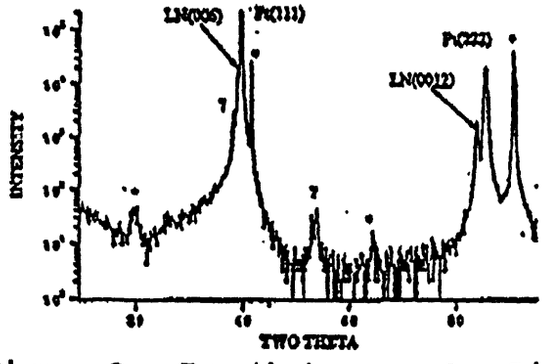

Figure 9. Two theta scan for $LiNbO_3$ on sputtered Pt on c-axis sapphire (* represents sapphire).

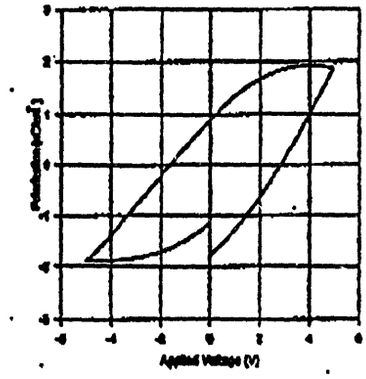

Figure 10. Polarization-voltage loop for $LiNbO_3$ film.

CONCLUSIONS

The solid source MOCVD technique (SSMD) has proven to be useful for the growth of technologically important electro-optic films. Impurity content of the films, particularly for iron which introduces photorefractive damage, is a factor of 30 lower than bulk $LiNbO_3$. The optical loss of $LiNbO_3$ on large area substrates is to date about 2 dB/cm at 633.2 nm for films as thin as 1175 Å. Initial measurements of polarization vs field confirm domain switching in these (001) oriented thin films. The ability of SSMD to grow large area uniform films at practical growth rates make this technique promising for further development in this field.

ACKNOWLEDGMENTS

We are indebted to Bruce Borsberry of Hewlett-Packard for design and construction of the single prism optical loss measurement, to Brady Sih of Stanford University for the differential scanning calorimetry results, and to Professor Angus Kingon of North Carolina State University, Michael Kautzky of Stanford University, and Paul Merchant of Hewlett-Packard for the sputtered (111) oriented platinum base electrode layers. The SIMS analysis was performed by John Turner and Dale Lefforge of Hewlett-Packard.

REFERENCES

1. R. Hiskes, S.A. DiCarolis, J.L. Young, S.S. Laderman, R.D. Jacowitz, and R.C. Taber, Appl. Phys. Lett.,59 (5), 606 (1991).

2. R. Hiskes, S.A. Dicarolis, R.D. Jacowitz, Z. Lu, R.S. Feigelson, R.K. Route, and J.L. Young, J. Cryst. Growth **128**, 781 (1992).

3. M.E. Cowher, T.O. Sedgwick, J. Landerman, J. Elect. Materials **3**, 621 (1974).

4. K. Zhang, E.P. Boyd, B.S. Kwak, A.C. Wright, and A. Erbil, Appl. Phys. Lett. **55**, 1258 (1989).

5. G. Malandrino, D.S. Richeson, T.J. Marks, D.C. DeGroot, J.L. Schindler, and C.R. Kanewurf, Appl. Phys. Lett. **58**, 182 (1991).

6. S.J. Duray, D.B. Buchholz, S.N. Song, D.S. Richeson, J.B. Ketterson, T.J. Marks, and R.P.H. Chang, Appl. Phys. Lett. **59**, 1503 (1991).

7. J. Zhao, C.S. Chern, Y.Q. Li, D.W. Noh, P.E. Norris, P. Zawadski, B. Kear, and B. Gallois, J. Cryst. Growth **107**, 699 (1991).

8. Z. Lu, R.S. Feigelson, R.K. Route, S.A. DiCarolis, R. Hiskes, and R.D. Jacowitz, J. Cryst. Growth **128**, 788 (1992).

9. K. Truman, Conductus, Inc., private communication.

10. G. Meng, G. Zhou, R.L. Schneider, B.K. Sarma, and M. Levy, Appl. Phys. Lett. **63**, 1981 (1993).

11. Strem Chemicals Inc., 7 Mulliken Way, Dexter Industrial Park, P.O. Box 108, Newburyport, MA 01950.

12. C. Houtman, D.B. Graves, and K.J. Jensen, J. Electrochem. Soc. **133**, 961 (1986).

13. J.D. Parsons, J. Cryst. Growth **116**, 387 (1992).

14. J.R. Carruthers and M. Grasso, J. Electrochem. Soc. **117**, 1427 (1970).

15. Z. Lu, R.S. Feigelson, R.K. Route, R. Hiskes and S.A. DiCarolis, these proceedings.

16. G.S. Hammond, D.C. Nonhebel, and C-W. S. Wu, Inorg. Chem. **2**, 73 (1963).

17. S. Schwyn, H.W. Lehmann, and R. Widmer, J. Appl. Phys. **72**, 1154 (1992).

18. D. Fork and G.B. Anderson, Appl. Phys. Lett. **63**, 1029 (1993).

19. A. Yamada, H. Tamada, and M. Saitoh, Appl. Phys. Lett. **61**, 2848 (1992).

20. R.A. Betts and C.W. Pitt, Electron. Lett. **21**, 960 (1985).

21. K. Nashimoto and M.J. Cima, Mat. Lett. **10** 348 (1991).

22. B.J. Curtis and H.R. Brunner, Mat. Res. Bull. 10, 515 (1975).

23. A.A. Wernberg, H.J. Gysling, A.J. Filo, and T.N. Blanton, Appl. Phys. Lett. 62, 946 (1993).

24. L.O. Svaasand, M. Eriksrud, G. Nakhen, and A.P. Gramde, J. Cryst. Growth 22, 230 (1974).

25. A. Rauber in Current Topics in Materials Science, volume 1, edited by E. Kaldis (1976) p. 481.

26. Radiant Technologies, Inc. 1009 Bradbury Drive SE, Albuquerque, NM 87106.

DATE
FILMED
2/7/94

END